Effect of thickness of antimony selenide film on its photoelectric properties and microstructure

Xin-Li Liu(刘欣丽)[1,3,5], Yue-Fei Weng(翁月飞)[1,3,5], Ning Mao(毛宁)[1,3,5], Pei-Qing Zhang(张培晴)[2,3,5], Chang-Gui Lin(林常规)[2,3,5], Xiang Shen(沈祥)[1,3,4,5], Shi-Xun Dai(戴世勋)[2,3,5], and Bao-An Song(宋宝安)[1,3,5,†]

[1] *Faculty of Electrical Engineering and Computer Science, Ningbo University, Ningbo* 315211, *China*
[2] *The Research Institute of Advanced Technologies, Ningbo University, Ningbo* 315211, *China*
[3] *Key Laboratory of Photoelectric Detecting Materials and Devices of Zhejiang Province, Ningbo* 315211, *China*
[4] *Ningbo Institute of Oceanography, Ningbo University, Ningbo* 315211, *China*
[5] *Engineering Research Center for Advanced Infrared Photoelectric Materials and Devices of Zhejiang Province, Ningbo* 315211, *China*

(Received 19 April 2022; revised manuscript received 15 July 2022; accepted manuscript online 5 August 2022)

Antimony selenide (Sb_2Se_3) films are widely used in phase change memory and solar cells due to their stable switching effect and excellent photovoltaic properties. These properties of the films are affected by the film thickness. A method combining the advantages of Levenberg–Marquardt method and spectral fitting method (LM–SFM) is presented to study the dependence of refractive index (RI), absorption coefficient, optical band gap, Wemple–DiDomenico parameters, dielectric constant and optical electronegativity of the Sb_2Se_3 films on their thickness. The results show that the RI and absorption coefficient of the Sb_2Se_3 films increase with the increase of film thickness, while the optical band gap decreases with the increase of film thickness. Finally, the reasons why the optical and electrical properties of the film change with its thickness are explained by x-ray diffractometer (XRD), energy dispersive x-ray spectrometer (EDS), Mott–Davis state density model and Raman microstructure analysis.

Keywords: antimony selenide films, photoelectric properties, Levenberg–Marquardt method and spectral fitting method (LM–SFM), microstructure

PACS: 78.20.Ci, 78.20.–e, 78.20.Bh **DOI:** 10.1088/1674-1056/ac8724

1. Introduction

Antimony selenide (Sb_2Se_3) has emerged as an alternative absorber material due to its high absorption coefficient, appropriate optical band gap, nontoxicity, low cost and earth-abundant.[1–3] It is the promising candidate for important applications in diverse areas such as solar energy conversion, thermoelectric cooling, photo detector technology, thermoelectric power generation and opto-electronics in the near-infrared region.[4] Particularly, it has been a promising absorber layer for solar cells and displays good photovoltaic properties.[5] With the development of magnetron sputtering (MS), thermal evaporation (TE), pulsed laser deposition (PLD) and other film preparation technologies, the Sb_2Se_3 has attracted more and more attention in the field of solar cells in recent years.[6–8] The film thickness affects its optical, electrical properties and microstructure. It is very important to find the law of film properties changing with its thickness for the preparation of high-quality optoelectronic devices.

The research on the Sb_2Se_3 thin films prepared by TE has been widely reported. M. M. Alligavathy *et al.* studied the structure, morphology and optical properties of the Sb_2Se_3 films prepared by TE.[9,10] Chen Chao *et al.* systematically analyzed the photovoltaic relevant physical properties of the Sb_2Se_3 films.[11] R. T. Ananth Kumar *et al.* compared the structure of Sb_2Se_3 films after annealing.[12] Researchers had also begun to pay attention to the properties of Sb_2Se_3 films prepared by PLD and MS. Yang Ke *et al.* researched the structure, morphology, composition and photoelectric properties of the Sb_2Se_3 films prepared by PLD.[13] Chen Shiming *et al.* and Liang Guangxing *et al.* discussed the material and photovoltaic properties of the Sb_2Se_3 films prepared by MS at different substrate temperatures.[14,15] Alapan Dutta *et al.* analyzed the influence of growth angle (0°–87° range) on the photoelectric properties of the Sb_2Se_3 thin films prepared by MS.[16] However, there still lacks of detailed and systematic study on the change of optical and electrical properties of the Sb_2Se_3 film with its thickness prepared by MS.

The optical and electrical properties of the Sb_2Se_3 films with different thicknesses prepared by MS are analyzed and studied systematically. Firstly, the method and principle of obtaining the properties of the films are presented, and Levenberg–Marquardt method and spectral fitting method (LM–SFM) calculation accuracy is analyzed by simulation. Then, the refractive index (RI), absorption coefficient and optical band gap of the Sb_2Se_3 films with different thicknesses prepared by MS are calculated by LM–SFM, and the variation laws of film properties with thickness are revealed. Finally,

†Corresponding author. E-mail: songbaoan@nbu.edu.cn
© 2023 Chinese Physical Society and IOP Publishing Ltd

energy dispersive x-ray spectrometer (EDS) and Raman spectroscopy are used to analyze the reason why the optical and electronic properties of the film change with its thickness.

2. Principle and simulation

2.1. Principle

The schematic diagram of accurately calculating the RI and absorption coefficient of the Sb_2Se_3 films is shown in Fig. 1. By optimizing the square root error between the calculated values $T_{\rm fit}$ and the measured values T, the RI and absorption coefficient of the film in the whole transmission spectrum can be obtained accurately. The detailed analyses are as follows.

The transmittance T of the film can be expressed as

$$T = \frac{Ax}{B - Cx\cos\varphi + Dx^2}, \tag{1}$$

where $A = 16n^2 s$, $B = (n+1)^3(n+s^2)$, $C = 2(n^2-1)(n^2-s^2)$, $D = (n-1)^3(n-s^2)$, $\varphi = 4\pi nd/\lambda$, $x = \mathrm{e}^{-\alpha d}$, λ is the wavelength, φ is the phase, n and s are the refractive indices of the film and substrate, respectively, d is the film thickness, α is the absorption coefficient of the film. The initial value of the absorption coefficient α_0 is calculated by using the following expression:

$$\alpha = \frac{1}{d}\ln\left(\frac{1}{T}\right). \tag{2}$$

Both d and n_0 can be calculated by SFM[17] and Cauchy model. T is the measured transmittance. Three calculated parameters d, n_0 and α_0 are substituted into Eq. (1) to obtain the calculated transmittance T_0, and the square root error e_0 between T_0 and T is calculated.

LM algorithm is used for global optimization to obtain n and α of thin films in strong absorption region. The iteration parameters $\Delta\alpha$ and Δn are calculated by following equation:

$$\Delta\alpha = g_\alpha/(H_\alpha + \mu I), \quad \Delta n = g_n/(H_n + \mu I), \tag{3}$$

where g_α is the first partial derivative of T with respect to α, g_n is the first partial derivative of T with respect to n, H_α is the Hessian matrix of α, H_n is the Hessian matrix of n, μ is the step size for optimization. The two optimized parameters are $\alpha = \alpha_0 + \Delta\alpha$, $n = n_0 + \Delta n$. The transmittance $T_{\rm fit}$ is fitting data from discrete calculated values. These two parameters α and n can be calculated accurately by continuously optimizing the error e between $T_{\rm fit}$ and T through iterative calculation.

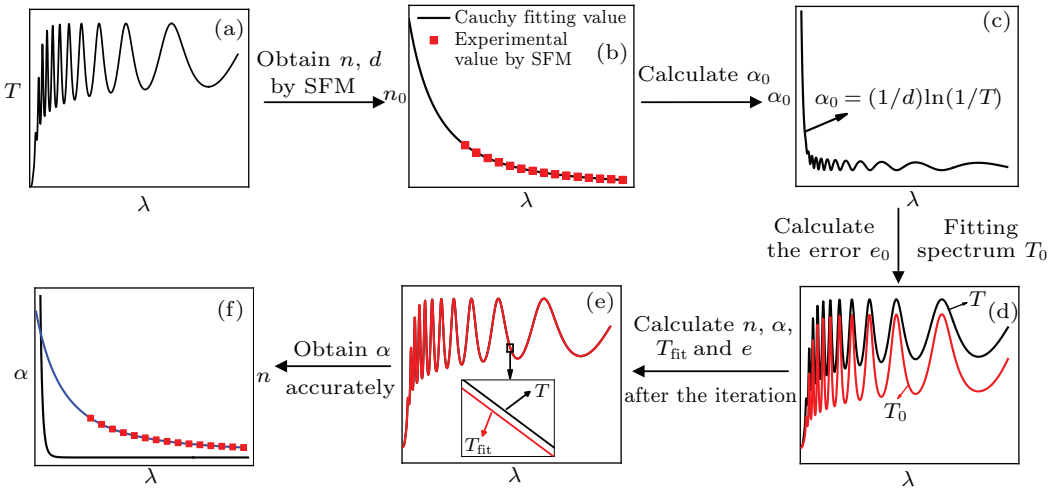


Fig. 1. Schematic diagram of the LM–SFM. (a) Transmission spectrum. (b) Initial RI. (c) Initial absorption coefficient. (d) The calculated value T_0 and the measured value T. (e) Transmittance error e. (f) RI and absorption coefficient.

2.2. Simulation

The effectiveness and reliability of the LM–SFM are analyzed by simulation. The film parameters are from Ref. [18]. As follows: $s = 1.51$, $d = 1000$ nm, $n_{\rm tr} = \frac{3\times10^5}{\lambda^2} + 2.6$, $\lg a_{\rm tr} = \frac{1.5\times10^6}{\lambda^2} - 8$. The transmittance $T_{\rm tr}$ of the film is obtained by using Eq. (1). The film thickness is calculated by SFM, which is 999.9 nm. The n_0 of the film in the absorption region is fitted by Cauchy dispersion model, the fitting equation is as follows:

$$n_0 = 2.6001 + \frac{3.0023\times10^5}{\lambda^2}. \tag{4}$$

The simulation results are shown in Fig. 2. Figures 2(a)–2(c) show the calculated absorption coefficient, refractive index and transmittance, respectively. Figures 2(d)–2(f) depict the corresponding calculation errors, respectively. It can be seen from the figure that n and α in the whole transmission spectrum are accurately calculated. The calculation accuracy of the refractive index and the absorption coefficient is better than 0.03% and better than 3% by using the LM–SFM, respectively.

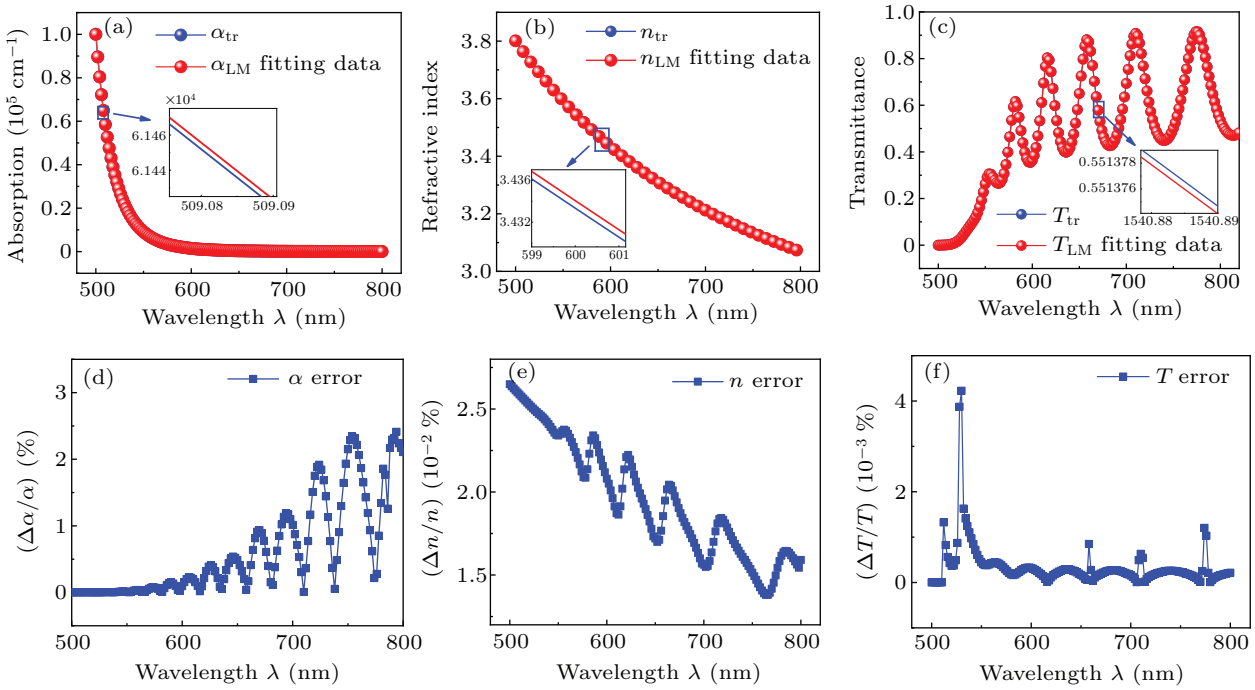


Fig. 2. Simulation results. (a) Absorption coefficient. (b) RI. (c) Transmission spectra. (d) Absorption coefficient error. (e) RI error. (f) Transmittance error.

3. Experiment

3.1. Preparation of thin films

The glass target was prepared by using the traditional melting quenching method. In this experiment, high purity Sb and Se powders was used as raw materials. They were weighed accurately on an electronic balance according to the designed composition ratio and placed in quartz glass tubes. The purity of Sb and Se was 99.999%. The quartz tube with raw material was pre-heated to 100 °C to remove the water in the raw material. Then vacuumed the quartz tube until the vacuum degree was below 10^{-3} Pa. It was fused with hydrogen and oxygen flame and put into the rocking furnace and heated to 1000 °C for 10 h, then took out and quenched in water. After glass demolding, it was annealed slowly to room temperature in the annealing furnace. Finally, the glass was processed into a double-sided polished sample with the size of Φ76.2 mm×3 mm as the target material.

The Sb_2Se_3 thin films were deposited on the SiO_2 glass substrate by magnetron sputtering. During the preparation process, the chamber pressure was evacuated to lower than 10^{-5} Pa, Ar gas flow was 50 sccm and then the sputtering pressure was 0.5 Pa. The sputtering power was maintained at 40 W. The substrate upon which thin film was deposited and rotated at a speed of 20 r/min and maintained at 25 °C during the deposition. The sputtering time was 15 min, 35 min, 55 min, 75 min and 100 min, respectively. After preparation, the film was placed in a vacuum annealing furnace and annealed at 100 °C for 1 h.

3.2. Characterization of thin films

The transmission spectra of the films was measured by spectrophotometer (PerkinElmer Lambda 950), and the spectral range was 500 nm–2500 nm. The phase x-ray diffractometer (XRD) of Bruker D2 and micro-Raman spectrometer were used to measure and analyze the structure of the thin films. The Raman laser wavelength was 785 nm and the laser power was 0.1 MW. The compositions of the thin film samples were characterized by using an EDS installed in a Tescan VEGA3 SB-Easyprobe scanning electron microscope. All tests were conducted at room temperature.

4. Results and discussion

4.1. Optical properties of Sb_2Se_3 thin films

Figure 3(a) is the transmission spectra of the film. The initial RI n_0 of the Sb_2Se_3 thin films in absorption region is calculated by SFM and Cauchy dispersion model, and obtained initial absorption coefficients α_0 by Eq. (2). Then, according to the LM method, continuously optimize the error between calculated value T_{fit} and measured value T through iterative calculation. When T_{fit} is consistent with T, α and n are obtained accurately as shown in Fig. 3(b). The T_{fit} and T in absorption region are compared as shown in Fig. 3(c). Figure 3(d) is the deviation between T_{fit} and T in absorption region and the overall deviation is less than 1.5%.

The optical parameters of the films are measured and calculated as shown in Fig. 4. Figure 4(a) is the transmission spectra of the films which shows that the absorption cutoff edge moves to the long-wave direction with the increase of

the thicknesses of the thin films. Figure 4(b) shows the change of film RI with wavelength. The results indicate that the RI of the thin film decreases with the increase of wavelength and increases with the increase of film thickness at the same wavelength. The absorption coefficients α of the Sb_2Se_3 thin films of different thicknesses are shown in Fig. 4(c) which shows that, at lower wavelength values, and before the absorption edge of samples, the absorption coefficient α has higher values. These high α-values attribute to the resonance impacts which may occur between the incident photons and the electronic polarizability. Also, the α for all film samples are found to decrease dramatically at the absorption edge, which due to the occurrence of coupling of the electrons. The absorption depends mainly on the photon energy $h\nu$ according to the Urbach relation

$$\alpha = a_0 \exp\left(\frac{h\nu}{E_u}\right), \tag{5}$$

where a_0 is a constant and E_u is the width of localized tail states which represents the degree of disorder in the non-crystalline material.[32] $h\nu$ decreases as the wavelength broadens, so α decreases as the wavelength broadens.

Based on the magnitudes of α, the extinction coefficients k of the Sb_2Se_3 films can be deduced from the following relation:

$$k = \frac{\alpha\lambda}{4\pi}. \tag{6}$$

The k of the Sb_2Se_3 thin film is shown in Fig. 4(d). It can be seen that k decreases with the increase of wavelength and increases with the increase of thin film thickness.

The relation between absorption coefficient and optical band gap for direct transition is given by the Tauc equation

$$(\alpha h\nu)^{1/2} = B^{1/2}(h\nu - E_g), \tag{7}$$

where $h\nu$ is the photon energy, E_g is the optical band gap, and $B^{1/2}$ is the Tauc parameter. Plotting $(\alpha h\nu)^{1/2}$ against $h\nu$ and extending the linear part to $(\alpha h\nu)^{1/2} = 0$ to calculate E_g of the thin films, as shown in Fig. 4(e). The results illustrate that the E_g decreases gradually with the thickness of the film increases. Tauc parameter is the slope of the line after linear fitting. E_g and Tauc values are listed in Table 1.

In addition, RI dispersion values of the Sb_2Se_3 thin films with different thicknesses have also been analyzed using the single oscillator model expressed by the Wemple and DiDomenico (WDD) as follows:[19,20]

$$n^2 = 1 + \frac{E_0 E_d}{E_0^2 - (h\nu)^2}, \tag{8}$$

where E_0 is the single oscillator energy. E_d is the dispersion energy. Plotting $(n^2-1)^{-1}$ against $(h\nu)^2$ and fitting a straight line with a slope of $(E_0E_d)^{-1}$ and an intercept of (E_0/E_d), as shown in Fig. 4(f). The calculated parameters E_0 and E_d are listed in Table 1. It is clear from this table that both E_0 and E_d decrease with the increase of film thickness. According to the WDD model, the static RI n_0 and the static dielectric constant ε_∞ of the film are calculated, which are summarized in Table 1 and their values increase with the increase of the film thickness.

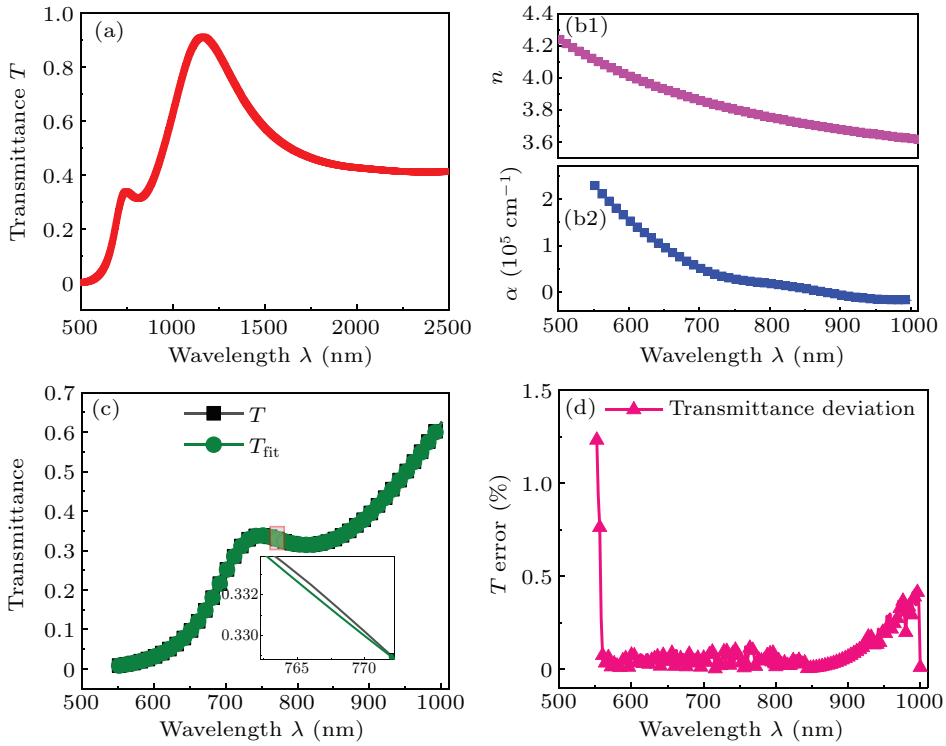


Fig. 3. The RI and absorption coefficient α of the Sb_2Se_3 film by LM–SFM. (a) Transmission spectrum. (b) The RI and α. (c) Comparison of T_{fit} and T. (d) The deviation between T_{fit} and T.

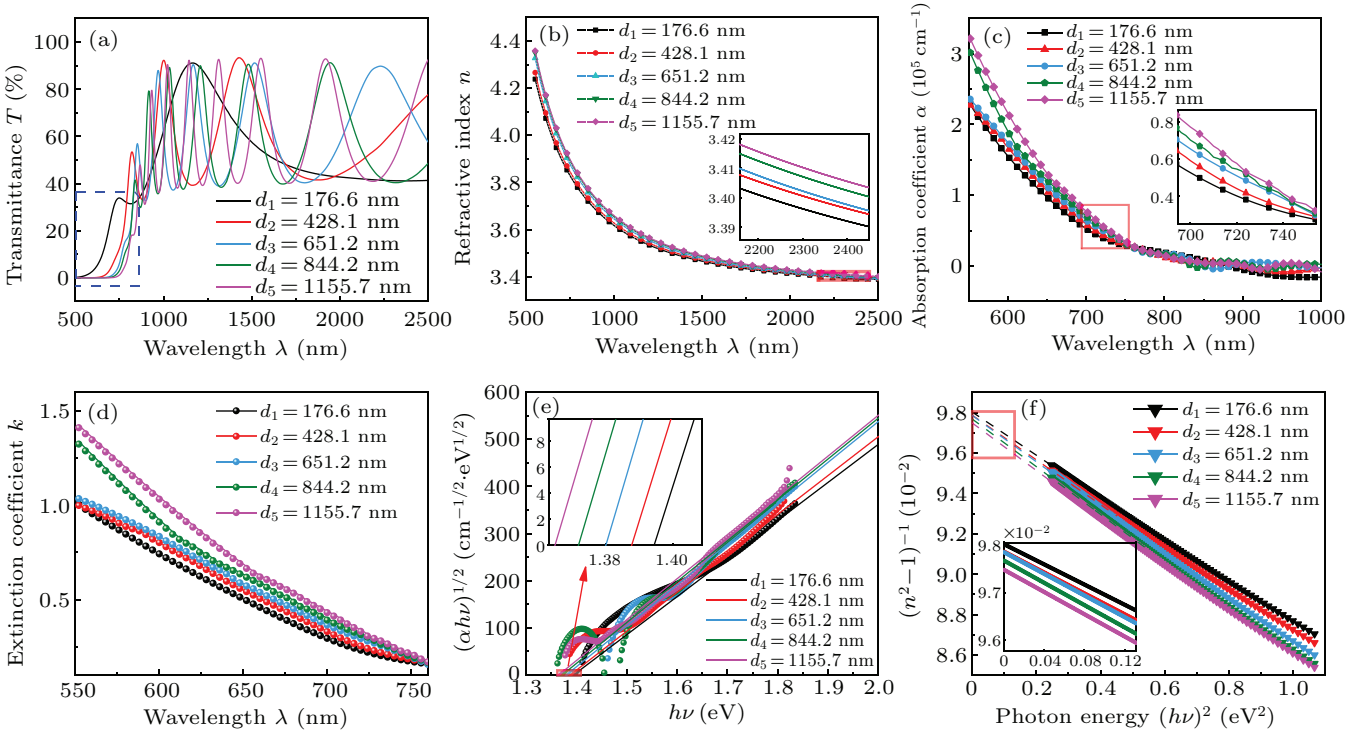


Fig. 4. Optical properties of the Sb_2Se_3 thin films. (a) Transmission spectrum. (b) RI. (c) Absorption coefficient. (d) Extinction coefficient. (e) Optical band gap. (f) The dependence of $(n^2-1)^{-1}$ on $(h\nu)^2$.

Table 1. Optical parameters of the Sb_2Se_3 films of different thicknesses.

Thickness (nm)	E_d (eV)	E_0 (eV)	E_g	$B^{1/2}$	n_0	ε_∞
176.6	30.921	3.031	1.395	808.142	3.3469	11.2016
428.1	30.481	2.983	1.388	825.957	3.3494	11.2182
651.2	29.674	2.900	1.380	867.422	3.1515	11.2324
844.2	29.492	2.881	1.372	867.597	3.3521	11.2367
1155.7	29.453	2.871	1.365	867.694	3.3554	11.2588

4.2. Electrical properties of the Sb_2Se_3 thin films

In the transparent region, the dielectric constant is attributed to free and bound electrons. According to the Spitzer–Fan model, the lattice dielectric constant, ε_L, and the ratio of the charge carrier concentrations to the effective mass, N_{opt}/m^*, of the Sb_2Se_3 films with different thicknesses are estimated[21,22]

$$n^2 = \varepsilon_L - \left(\frac{e^2}{4\pi^2 c^2 \varepsilon_0}\right)\left(\frac{N_{opt}}{m^*}\right)\lambda^2, \tag{9}$$

where e is the electronic charge, c is the speed of light, and ε_0 is the dielectric constant of vacuum. The magnitudes of ε_L and N_{opt}/m^* of the Sb_2Se_3 thin films with different thicknesses are estimated by plotting the relation between n^2 and λ^2, the values of ε_L and N_{opt}/m^* can be evaluated from the slopes and intercepts, respectively, and are listed in Table 2.

Table 2. Electrical parameters of the Sb_2Se_3 thin films of different thicknesses.

Thickness (nm)	ε_L	N_{opt}/m^* (10^{46} g·cm^3)	ω_p (10^{13}/s)
176.6	11.895	8.292	4.63
428.1	11.983	9.620	4.99
651.2	11.999	9.713	5.01
844.2	12.052	10.150	5.12
1155.7	12.079	10.281	5.15

Figure 5(a) displays the relation curve between the ε_L and N_{opt}/m^*, there is an exponential relationship between the ε_L and N_{opt}/m^*.

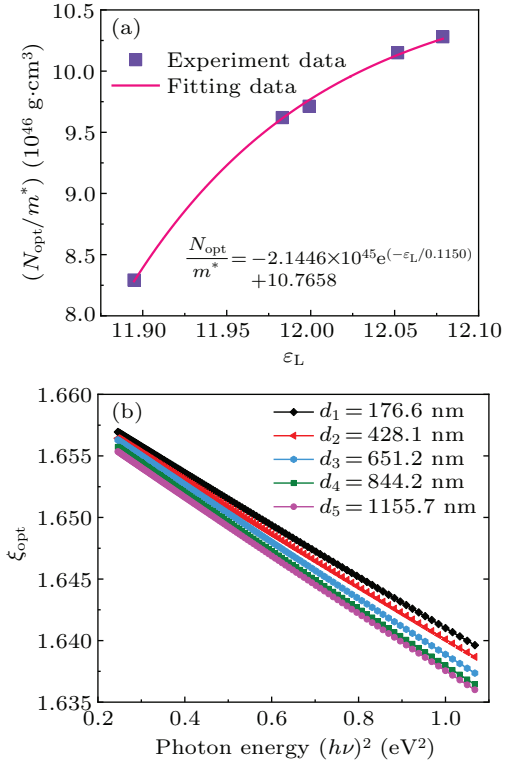


Fig. 5. Electrical properties of the Sb_2Se_3 thin films. (a) The dependence of N_{opt}/m^* on ε_L of the Sb_2Se_3 thin films. (b) The dependence of ξ_{opt} on $(h\nu)^2$ of the Sb_2Se_3 thin films.

Optical electronegativity, ξ_{opt}, is an important parameter to reflect the tendency of an atom to attach electrons from an-

ionic bands. The ξ_{opt} of the Sb_2Se_3 films is estimated by[23]

$$\xi_{opt} = \left(\frac{A}{n}\right)^{1/4}, \tag{10}$$

where A is a constant with a magnitude of 25.54 and n is the RI. Figure 5(b) shows the dependence of the ξ_{opt} on the photon energy $(h\nu)^2$ of the Sb_2Se_3 thin films with different thicknesses, the ξ_{opt} decreases with the increase of photon energy and film thickness.

The plasma frequency ω_p is known as the frequency of the resonance of the electron free oscillations around their positions of equilibrium and is defined by[24]

$$\omega_p = \left(\frac{e^2 N_{opt}}{\varepsilon_0 \varepsilon_\infty m^*}\right)^{\frac{1}{2}}, \tag{11}$$

the results are listed in Table 2, the ω_p increases with the increase of the film thickness.

4.3. Structure analysis of Sb_2Se_3 thin films

Figure 6(a) shows the SAED and HRTEM images of the Sb_2Se_3 films with thickness of 176.6 nm. The SAED image shows that the film has characteristic of amorphous structure. Furthermore, there is no regular lattice fringe in the HRTEM image and XRD spectra without sharp peak, as shown in Fig. 6(c), which also indicates the film is amorphous. The wide and small ridges at low angle are due to the glassy properties of the glass substrate.[25] The broad peak becomes stronger with thickness, indicating a higher degree of short-range order.

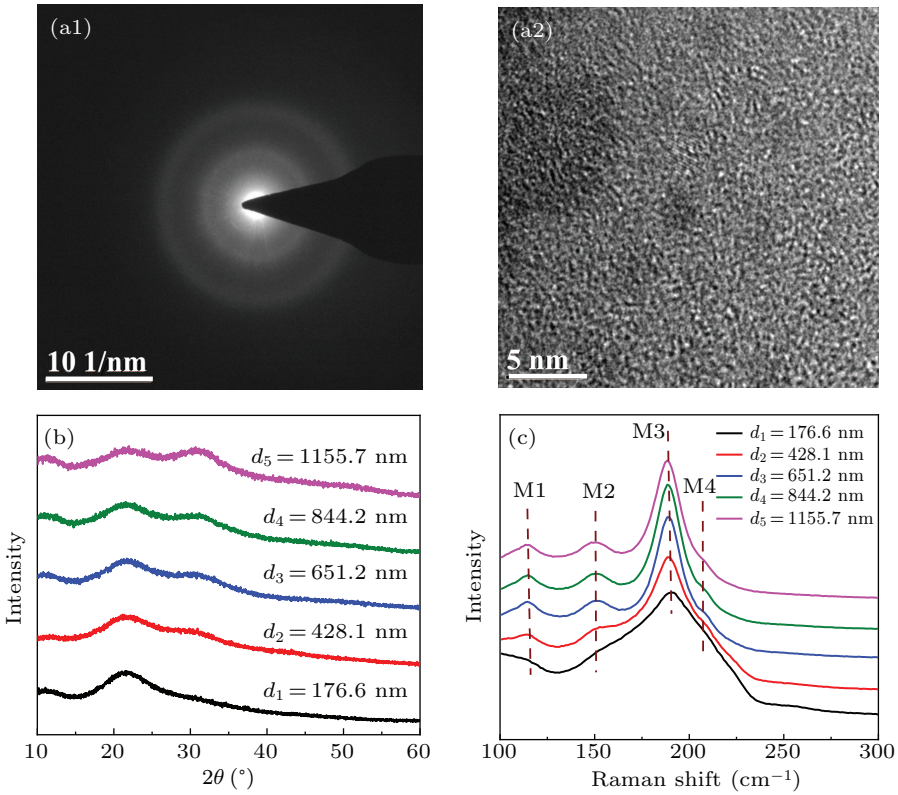


Fig. 6. Microscopy and spectroscopy of the Sb_2Se_3 thin films. (a1) SAED image of thickness 176.6 nm. (a2) HRTEM image of thickness 176.6 nm. (b) XRD spectra. (c) Raman spectra.

Although a higher thickness of the Sb_2Se_3 film still reveals an amorphous structure, the relaxation of internal strains and/or the homogenization of defect concentration between amorphous regions may occur,[26] which leads to fewer defects in the film and consequently a higher degree of short-range order. The components of the Sb_2Se_3 films with different thicknesses are measured by EDS. The results are given in Table 3, which shows that the relative content of Se decreases, and the relative content of Sb increases with the increase of film thickness. This is due to the easy evaporation and volatilization of Se. In the preparation process, the longer the sputtering time, the easier Se volatilizes.

Table 3. Components of the Sb_2Se_3 films with different thicknesses.

Thickness (nm)	Components (at.%)	
	Se	Sb
176.6	59.27	40.73
428.1	58.68	41.32
651.2	58.04	41.96
844.2	57.84	42.16
1155.7	56.15	43.85

The Raman spectra of the Sb_2Se_3 films with different thicknesses in Fig. 6(d) shows that the Raman peaks are mainly in M1:120 cm^{-1}, M2:153 cm^{-1}, M3:190 cm^{-1} and M4:210 cm^{-1}. The peak at 120 cm^{-1} is associated with the Se–Se bonds vibration, and the peak at 153 cm^{-1} is closely

related to the Sb–Sb bonds vibration between (Se_2Sb–$SbSe_2$) structural unit.[27–29] There is only one main peak at 190 cm^{-1} for the film with the thickness of 176.6 nm, mainly because the Se–Se bonds and Sb–Sb bonds are disordered at a lower thickness not easily to detect, the bonds get order as the thickness increases and Se–Se bonds and Sb–Sb bonds are observed.[30] The intensity of Sb–Sb bonds increases with the film thickness, which because the relative content of Sb increases with the increase of film thickness, resulting in the number of Sb–Sb bonds increases. The main Raman peak and the lower intensity Raman peaks are observed at 190 cm^{-1}. 210 cm^{-1} is assigned to the Sb–Se bonds stretching vibration in the $SbSe_{3/2-}$ pyramids.[30] $SbSe_{3/2-}$ pyramids are the basic structural unit of the Sb_2Se_3 phase.[31] With the increase of film thickness, the chemical bond changes from disorder to order, and the structure of the film tends to be stable, which is consistent with the XRD results and the slope of Tauc increases with the increase of thickness.

4.4. The dependence of optical and electrical properties of Sb_2Se_3 films on the film thickness

The dependence is shown in Fig. 7. As shown in Figs. 7(a) and 7(b), the n and α increase exponentially with the film thickness. Figure 7(c) shows that the E_g of these films and their thickness maintain a linear relationship. The above two exponential relationships and the linear relationship can be expressed as

$$n = -0.0416 \times e^{-d/1316.4787} + 3.4899, \tag{12a}$$

$$\alpha = 6.7651 \times 10^{-4} \times e^{(d+1144.4751)/888.2132} + 0.0132, \tag{12b}$$

$$E_g = -3.1785 \times 10^{-5} d + 1.4007. \tag{12c}$$

The refractive index depends on the density and the average polarizability of the film. As described by the Lorentz–Lorenz equation[32,33]

$$\frac{n^2-1}{n^2+2} = \frac{4\pi}{3} \cdot \frac{N_A \rho}{M} a, \tag{13}$$

where N_A is the Avogadro constant, M represents the molar mass, ρ represents the density, and a represents the average polarizability. With the increase of film thickness, the relative content of Sb increases, while that of Se decreases. Sb cation has higher polarizability than that of other cations, so the RI of the film increases with the thickness of the film.

Raman analysis shows that the film is more orderliness with film thickness, the greater the orderliness and the smaller band-tail width energy E_u. Equation (5) shows that at the same wavelength, E_u decreases with film thickness, but α increases. The decrease of the E_g with film thickness can be explained by the state density model proposed by Mott and Davis,[34] which shows that the localized state width near the mobility edge is strongly depended on the degree of disorder and the presence of defects in the amorphous structure. The increase of Sb relative content leads to the increase of local state concentration. As the electronegativity of Sb is lower than Se, the band tail and band gap decrease, and the localized states width increases with the increase of Sb relative content.

It is known that the Tauc parameter is a measure of the disorder in the thin films, and the smaller the $B^{1/2}$ is, the disorder will be. Figure 7(d) shows that $B^{1/2}$ increases with film thickness, indicating the orderliness of the film increases. Meanwhile, the increase of heteropolar bond in Raman spectrum also indicates the increase of the order degree of the film.[6,30] When the thickness is greater than 500 nm, $B^{1/2}$ does not change significantly with the increase of thickness, indicating that thickness has little influence on the internal disorder degree of films with thickness greater than 500 nm.

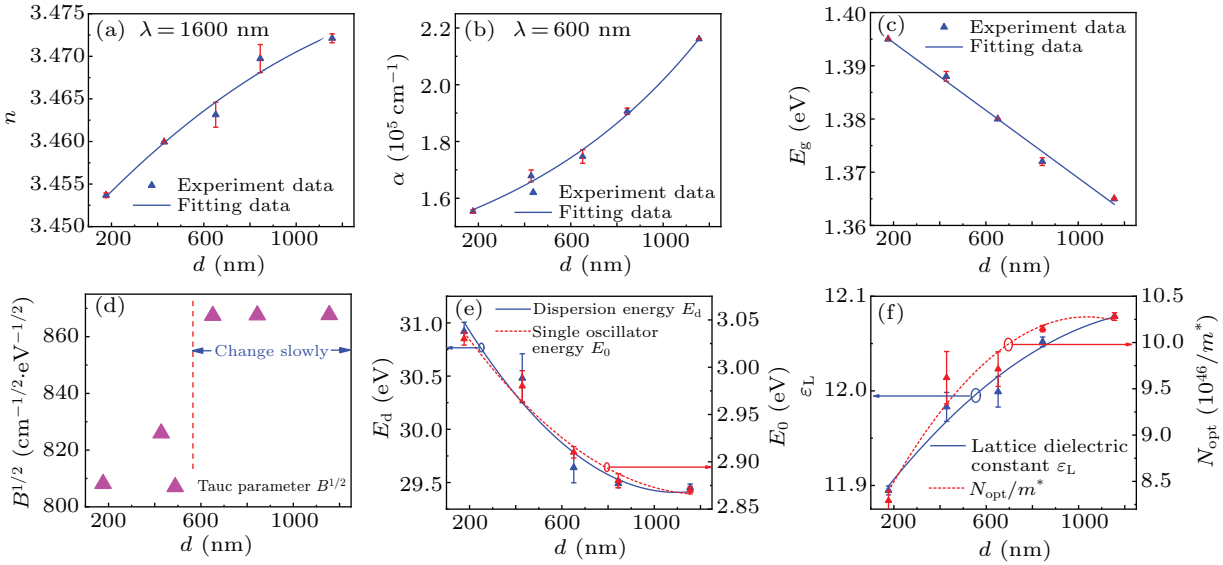


Fig. 7. The dependence of optical and electrical properties of the Sb_2Se_3 films on the film thickness. (a) n changes as a function of d. (b) α changes as a function of d. (c) E_g changes as a function of d. (d) $B^{1/2}$ changes as a function of d. (e) E_d and E_0 change as a function of d. (f) ε_L and N_{opt}/m^* change as a function of d.

The dependence of dispersion energy E_d and single oscillator energy E_0 on the thickness is displayed in Fig. 7(e). The results show that both of them decrease with the increase of the film thickness. Figure 7(f) shows that the relationship between the ε_L, the N_{opt}/m^* and film thickness d. Both of them increase with the increase of film thickness. This is because the increase of Sb leads to the decrease of the density of strong heteropolar bonds in the film, while the density of weak monopole bonds (such as Sb–Sb bonds) increases. Weaker bonds respond more easily to electric fields than that of stronger bonds, so as the relative Sb content increases, the density of weak bonds increases, leading to dielectric constant increases.

5. Conclusion

The optical and electrical properties of the Sb_2Se_3 films with the thicknesses ranging from 100 nm to 1200 nm are studied in detail by using the LM–SFM proposed in this paper. The thickness d and optical constants n, k, α, E_g are calculated accurately, the WDD parameters (E_0 and E_d) are also estimated. The dielectric constant ε_L, optical electronegativity ξ_{opt}, plasma frequency ω_p and the ratio of the charge carrier concentrations to the effective mass N_{opt}/m^* of the Sb_2Se_3 films with different thicknesses have also been obtained. The results show that n and α increase exponentially with the increase of the film thickness. The E_g of the film and its thickness maintain a linear relationship. When the film thickness is greater than 500 nm, Tauc parameters remain almost unchanged with the increase of film thickness. The WDD parameters decrease and N_{opt}/m^* increases with the increase of film thickness respectively. Finally, XRD, EDS and Raman spectra analysis indicate that with the increase of the film thickness, the relative content of Se decreases, and the relative content of Sb increases, which is the main reason why the optical and electrical properties change with the thickness. The results lay a foundation for further application of the Sb_2Se_3 thin films in phase change memory and solar cells.

Acknowledgements

Project supported by the National Natural Science Foundation of China (Grant Nos. 62075109, 62135011, 62075107, and 61935006) and K. C. Wong Magna Fund in Ningbo University.

References

[1] Koç F and Sahin M 2019 *Appl. Phys. A* **125** 1
[2] Němec P, Olivier M, Baudet E, Kalendoá A, Benda P and Nazabal V 2014 *Mater. Res. Bull.* **51** 176
[3] Saritha K, Rasool S, Ramakrishna Reddy K T, Saad A M, Tivanov M S, Tikoto S E, Korolik O V and Gremenok V F 2019 *Appl. Phys. A* **125** 704
[4] Kim I 2000 *Mater. Lett.* **43** 221
[5] Ghosh S, Moreira M V B, Fantini C and González J C 2020 *Sol. Energy* **211** 613
[6] Hu X, Tao J, Chen S, Xue J, Weng G, Kaijiang, Hu Z, Jiang J, Chen S, Zhu Z and Chu J 2018 *Sol. Energ. Mat. Sol. C.* **187** 170
[7] Liu X, Chen J, Luo M, Leng M, Xia Z, Zhou Y, Qin S, Xue D J, Lv L, Huang H, Niu D and Tang J 2014 *ACS Appl. Mater. Inter.* **6** 10687
[8] Yuan C, Zhang L, Liu W and Zhu C 2016 *Sol. Energy* **137** 256
[9] Malligavathy M, Ananth Kumar R T, Das C, Asokan S and Pathinettam Padiyan D 2015 *J. Non-Cryst. Solids* **429** 93
[10] El Radaf I M 2019 *Appl. Phys. A* **48** 6480
[11] Chen C, Bobela D C, Yang Y, Lu S, Zeng K, Ge C, Yang B, Gao L, Zhao Y, Beard M C and Tang J 2017 *Frontiers of Optoelectronics* **10** 18
[12] Malligavathy Rajakumar M, Ananth Kumar R T and Pathinettam Padiyan D 2019 *Energ. Source. Part A* **429** 93
[13] Yang K, Li B and Zeng G 2020 *Superlattice. Microst.* **145** 106618
[14] Chen S, Hu X, Tao J, Xue J, Weng G, Jiang J, Shen X and Chen S 2019 *Appl. Opt.* **58** 2823
[15] Liang G X, Zheng Z H, Fan P, Luo J T, Hu J G, Zhang X H, Ma H L, Fan B, Luo Z K and Zhang D P 2018 *Sol. Energ. Mat. Sol. C.* **174** 263
[16] Dutta A, Singh R, Srivastava S K and Som T 2019 *Sol. Energy* **194** 716
[17] Mao N, Song B, Pan L, Liu X, Lin C, Zhang P, Shen X and Dai S 2021 *Opt. Express* **29** 29329
[18] More J J 1978 *Funct. Anal. Appl.* **630** 105
[19] DrDomenico M and Wemple S H 1969 *J. Appl. Phys.* **40** 720
[20] Wemple S H and DiDomenico M 1971 *Phys. Rev. B* **3** 1338
[21] El-Bana M S, El Radaf I M, Fouad S S and Sakr G B 2017 *J. Alloy. Compd.* **705** 333
[22] Sharma P, El-Bana M S, Fouad S S and Sharma V 2016 *J. Alloy. Compd.* **667** 204
[23] Reddy R R, Rama Gopal K, Narasimhulu K, Reddy L S S, Kumar K R, Reddy C V K and Ahmed S N 2008 *Opt. Mater.* **31** 209
[24] Tichý L, Tichá H, Nagels P, Callaerts R, Mertens R and Vlčeka M 1999 *Mater. Lett.* **39** 122
[25] Hassanien A S and Sharma I 2019 *J. Alloys Compd.* **798** 750
[26] Tsai D C, Chang Z C, Kuo B H, Wang Y H, Chen E C and Shieu F S 2018 *J. Alloys Compd.* **743** 603
[27] Chee H L, Rui H, Wang Z H, Richard L J Q, Ajay K, Conor D, Ben B, T E Kidd, Chancey C C, Mohan Sankaran R and Xuan P A G 2013 *ECS Solid State Lett.* **5** 4337
[28] Shongalova A, Correia M R, Teixeira J P, Leitão J P, González J C, Ranjbar S, Garud S, Vermang B, Cunha J M V, Salomé P M P and Fernandes P A 2018 *Sol. Energ. Mat. Sol. C.* **187** 219
[29] Ivanovaa Z G, Cernoskovab E, Vassilevc V S and Boycheva S V 2003 *Mater. Lett.* **57** 1025
[30] Li Z, Chen X, Zhu H, Chen J, Guo Y, Zhang C, Zhang W, Niu X and Mai Y 2017 *Sol. Energ. Mat. Sol. C.* **161** 190
[31] Lu Y, Song S, Shen X, Wu L, Song Z, Liu B, Dai S and Nie Q 2013 *ECS Solid State Lett.* **2** P94
[32] Pan L, Song B, Mao N, Xiao C, Lin C, Zhang P, Shen X and Dai S 2021 *Opt. Commun.* **496** 127123
[33] Urbach F 1953 *Phys. Rev.* **92** 1324
[34] Mott N F, Davis E A and Weiser K 1972 *Phys. Today* **25** 55